

# Demonstration of near-infrared open-path absorption spectroscopy for water vapor and temperature monitoring during structure-to-structure fire spread experiments

ERIN E. MCCAUGHEY,<sup>1</sup> MONICA M. FLORES,<sup>1,2</sup> CHRISTOPHER U. BROWN,<sup>3</sup>  
ALEXANDER MARANGHIDES,<sup>3</sup> J. HOUSTON MILLER,<sup>1</sup> AND D. MICHELLE BAILEY<sup>3,\*</sup> 

<sup>1</sup>George Washington University, Washington, D.C. 20052, USA

<sup>2</sup>Current address: National Institute of Standards and Technology, Gaithersburg, Maryland 20899, USA

<sup>3</sup>National Institute of Standards and Technology, Gaithersburg, Maryland 20899, USA

\*michelle.bailey@nist.gov

Received 16 September 2025; revised 11 December 2025; accepted 12 January 2026; posted 13 January 2026; published 13 February 2026

With increasing threats from wildfires in wildland urban interface (WUI) areas, novel approaches for the characterization of fire dynamics and their interactions with built structures have accelerated. Here, we demonstrate an open-path, near-infrared laser absorption system for stand-off measurement of water vapor mole fraction and gas-phase temperature. The system was deployed along two optical paths during structure-to-structure fire spread experiments at the National Institute of Standards and Technology. Initial demonstration of the system was completed from March 2024 through May 2024 in the National Fire Research Laboratory, to assess whether open-path tunable diode laser absorption spectroscopy (TDLAS) can operate reliably under the challenging, smoke-laden, and rapidly evolving conditions of WUI-relevant fire exposures. Data were collected before ignition, during test burns, and throughout fire suppression. The system operates near 1393 nm with a typical signal-to-noise ratio exceeding 180. Results show increased temperature and water vapor mole fraction following fuel ignition, as well as variations related to fire-resistant eave vent activation times. These results highlight that open-path TDLAS is a viable nonperturbing measurement approach that can improve understanding of heat and gas flow for future large-scale fire studies, which can contribute to the enhancement of fire safety, building codes, and associated test methods. © 2026 Optica Publishing Group. All rights, including for text and data mining (TDM), Artificial Intelligence (AI) training, and similar technologies, are reserved.

<https://doi.org/10.1364/AO.578869>

## 1. INTRODUCTION

In recent decades, wildfires have grown more frequent and severe across North America and globally. One of the most concerning trends is the increasing impact of wildfires on the wildland-urban interface (WUI), areas where human development meets undeveloped wildland. According to the National Interagency Fire Center, the long-term average annual burned area from wildfires has nearly doubled from 3.3 million acres in the 1990s to 7.0 million acres since 2000 [1]. This rise is driven by climate-related factors, including increasing global temperatures [2], lower humidity, and more frequent, severe storms that result in a higher number of lightning-induced ignitions. Compounding this issue is the rapid expansion of communities into the fire-prone WUI regions. As of 2021, approximately 49 million homes were located within WUI zones [3], placing them at high risk. Numerous U.S. states have experienced their largest or most destructive WUI fires since 2018, including California,

Oregon, Washington, Colorado, New Mexico, Hawaii, and Tennessee. As a result of this growing threat, research focused on WUI fires has significantly expanded in scope and urgency.

This paper presents the development and initial demonstration of an open-path tunable diode laser absorption spectroscopy (TDLAS) system used to measure water vapor mole fraction and gas-phase temperature in two paths simultaneously during WUI fire spread experiments conducted at the National Fire Research Laboratory (NFRL) at the National Institute of Standards and Technology (NIST). The experimental burn series discussed here [4,5] aimed to better understand the resilience of structures in WUI fires, specifically how structures equipped with “fire-resistant” eave vents perform when faced with varied fire exposures. The vents used in this study incorporate multiple protective measures: mesh layers to prevent pests and fire embers from entering the structure, and a self-sealing intumescent coating designed to prevent the

transfer of heat and hot gases from passing from the exterior to the interior of the structure. Chapter 7A of the California Building Standards Code mandates that attic and eave vents resist the intrusion of flames and embers in compliance with ASTM E2886 standards [6], although this fire resistance may be achieved using various design features other than an intumescent coating. The broader goal of this experimental series is to inform those concerned with fire safety, building codes, and testing methodologies that may enhance structure resilience in critical WUI zones, while this paper focuses more specifically on demonstrating that open-path TDLAS can be a promising technique for use in similar fire studies.

The relationship and interaction between water and fire is complex. As a primary product of the combustion of hydrocarbon materials, which act as fuels, concentrations of water in structure fires can be expected to be elevated. However, the presence of a high-water vapor content at elevated temperatures poses unique challenges for fire diagnostics. While various instruments and techniques exist for measuring temperature and gases in fire environments, the conventional tools used to determine moisture levels, such as humidity sensors like hygrometers or psychrometers, typically have response times ranging between a few seconds to several minutes, making them unsuitable for high-temperature environments when a rapid response time is required [7–10]. Additionally, probes or sensors requiring *ex situ* analysis are intrusive and may have long-time averages due to gas mixing in the lines, introducing more temporal and spatial uncertainty into experimental results [11]. In contrast, TDLAS provides a less intrusive, *in situ* method for gas-phase diagnostics with high sensitivity, fast response time, and the need for minimal calibration. TDLAS enables measurements of trace gases, such as water vapor, over long path lengths without disturbing the combustion environment, making it uniquely suited for large-scale experiments [7]. This measurement approach preserves the integrity of the flame, smoke, and ventilation flow fields, which is essential to evaluating the performance of fire-resistant materials and structures under realistic conditions. It also allows for compact and flexible designs that allow for physical separation of electronics and equipment from the harsh environments under study. The capability to measure water vapor concentrations at unknown, elevated temperatures has been recognized by the Society of Fire Protection Engineers (SFPE) as essential to improve hazard assessment for occupants who may be trapped inside during a structure fire. According to the SFPE handbook, air or smoke with high water vapor content and high thermal capacity of latent heat is dangerous at higher temperatures and may cause burns throughout the respiratory tract [12].

TDLAS-based sensors have been widely applied to atmospheric monitoring, industrial process control, and combustion diagnostics. In fire detection, they have become increasingly used to monitor early markers of combustion, such as CO and CO<sub>2</sub> [13–15], in structures. This technique has been successfully used in high-temperature, optically thick environments like furnaces and power plants, where dense smoke and particulate matter present significant measurement challenges [7,16–18]. Moreover, TDLAS has demonstrated clear value in scenarios when visual access to the fire is limited, such as in fire extinction studies within enclosed backdraft chambers,

where traditional diagnostics rely heavily on visual observations or multiple instruments (thermocouples, heat flux gauges, commercial gas analyzers, etc.) with low temporal resolution [19]. By providing robust, nonperturbing measurements in extreme conditions, TDLAS stands out as a critical tool for experimental fire measurements that provides fast response time and measurement precision.

This paper demonstrates the use of open-path TDLAS technology for additional applications in large-scale fire spread experiments, where simultaneous measurements of temperature and gas amount fractions in multiple paths are critical to understanding the dynamics of the overall experimental system. Key to this approach is achieving a high signal-to-noise ratio and robust data throughput, enabling reliable monitoring under challenging experimental conditions. While implementing open-path TDLAS in such environments presents technical challenges such as interference from particulates and rapidly changing conditions, our results show these obstacles can be effectively managed, supporting the broader application of this technique in fire research.

## 2. EXPERIMENTAL SETUP

### A. Sensor Design

The overall instrument design follows the design from previous field demonstrations [20] and can be seen in Fig. 1. Measurements were performed using a fiber-coupled near-infrared (NIR) DFB laser centered around 1393 nm for the detection of water vapor mole fraction and the determination of gas-phase temperature of the experimental environment. The output wavelength was tuned via current to span the wavelength interval 1393.70–1393.42 nm ( $7175.13 - 7176.58 \text{ cm}^{-1}$ ) while the diode temperature was stabilized at 26.5°C.

A 50:50 fiber-optic splitter was used to transmit light onto two 10 m single-mode fiber patch cables to simultaneously transmit the NIR light to two identical optical launches as seen in Fig. 1(A). Each includes a two-channel design for co-aligning the NIR beam with a red visible laser using a long-pass dichroic mirror, which allows for easier alignment over the long path-lengths seen in Fig. 1. The launch and collection optics were covered in protective boxes to prevent excess heat from reaching optical components, and to prevent fire suppression water droplets from landing on electrical or optical components. The laser paths extended approximately 9 m (29.5 ft) to monitor water vapor mole fraction and gas-phase temperature along two regions of a target structure wall (see Section 5.A).

The two beams were aligned to strike 2-inch diameter 90° off-axis parabolic mirrors, which then focused the light onto fixed-gain InGaAs photodetectors in the collection optics enclosure, as seen in Fig. 1(B). A single-pass approach was used to avoid any additional beam steering caused by the smoke particulates and to simplify the maintenance of beam position in relation to the target structure. The response of the detectors was recorded using a Measurement Computing Corporation (MCC) USB-2020 digitizer (see Acknowledgment). The laser controller, function generator, and digitizer [Fig. 1(C)] were controlled via a custom Python script configured for

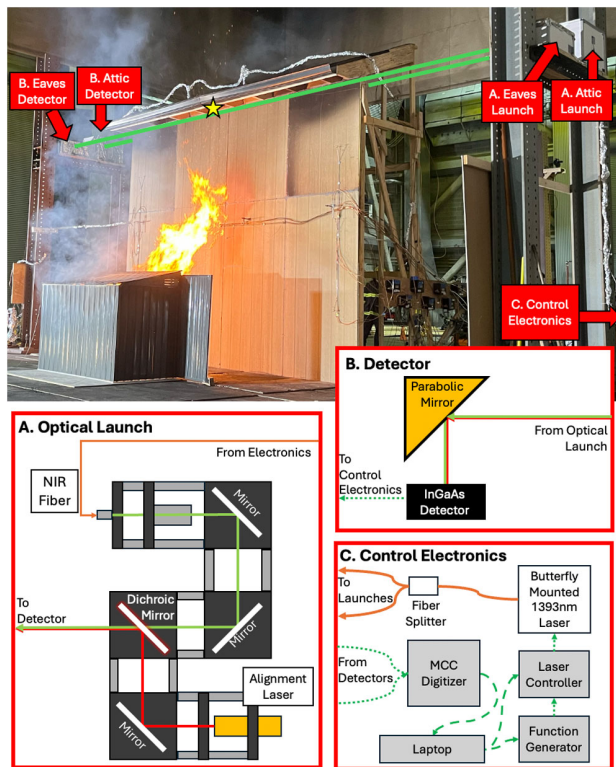


**Fig. 1.** Schematic of the instrument configuration for structure-to-structure fire spread experiments and the relative location of (A) optical launches, (B) detectors, and (C) control electronics in the experimental configuration. The green dashed and dotted lines represent digital and analog communications, respectively. Orange solid lines represent single-mode fibers used to carry NIR light to the launch optics. Green and red solid lines represent laser light. Cage-mounted launch optics, and collection mirrors and detectors sit on 30 cm by 30 cm square breadboards on opposite sides of the target structure. The eave vent location at the top of the target structure wall is indicated by a yellow star with the flame jet directed toward it.

single-spectrum collection, which limited the acquisition rate to approximately 7 Hz, or one spectrum every 143 ms.

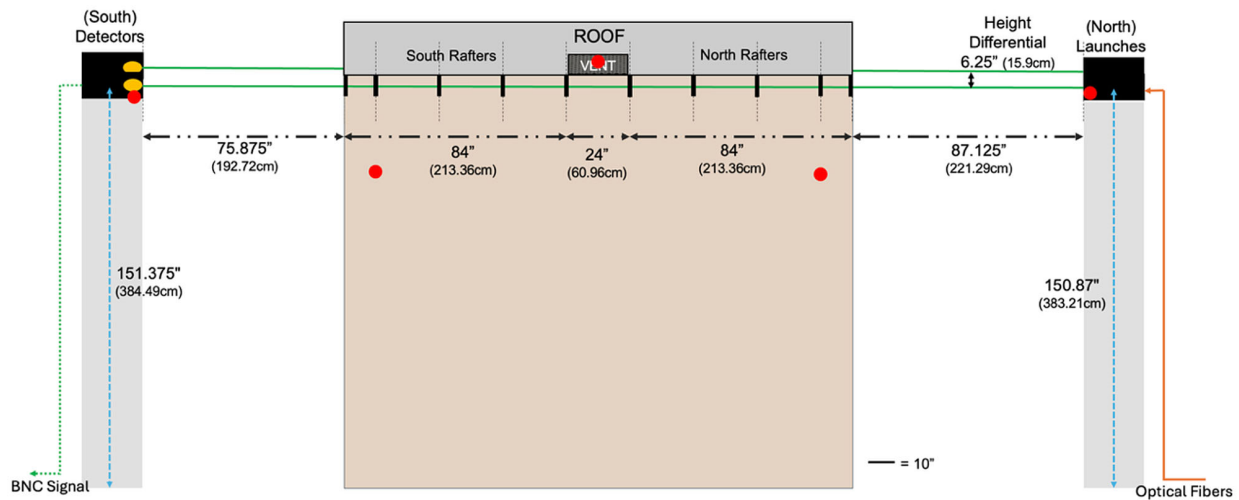


**Fig. 2.** A diagram of the laser instrument incorporated into the target structure set-up. The target structure is shown in the center with laser launch and collection platforms on either side. The total path lengths from laser launch to detector were approximately 901 cm (29.5 ft). Placements of the thermocouples (TCs) throughout the structure are marked with red circles. Black dot-dash lines represent measured segments of the path length.

## B. Test Infrastructure

The objective of the experimental burn series was to observe the performance of commercially available “fire-resistant” eave vents, which conform to Chapter 7A of the California Building Standards Codes and ASTM E2886 standards [6], specifically those designed with a self-sealing intumescent coating to prevent hot gases and embers from entering the interior of the structure. The target structure was designed to represent the façade of a single-story structure with the vent installed under the eaves of the roof at the top of the outer wall [approximately 4 m (13 ft) above the floor]. The wall was approximately 4.9 m (16 ft) wide. For the complete experimental design of the target structure and placement of the vents, see Refs. [4,5].

In this paper, the measured optical “eaves path” ran across the exterior of the target structure, closest to the fire, below the eave vent and rafter bays, and aimed to capture changes in the temperature and water vapor mole fraction in the uncontrolled flame environment. This pathlength was measured to be 901.69 cm (355.0 in). The “attic path” ran along the back side of the wall behind a plenum box and eave vent and was measured to be 901.06 cm (354.75 in) and aimed to capture the temperature and gas effects as the vent interacts with the fire. Path lengths were measured using a combination of direct physical measurements and verification with computer-aided designs of the target structure and laser platforms to ensure accuracy in the corresponding distances. The two paths were separated by approximately 81 cm (32 in). Compared to the eaves path, the attic path was elevated by 15.875 cm (6.25 in) to allow the beam to pass through concentrated gases exiting from the plenum box leading from the vent, as shown in Figs. 1 and 2.

Data were collected with the open-path system during 12 experimental burns in which noncombustible sheds of varying size and fuel loads (wood cribs) were burned. The sheds were placed at different separation distances from the target wall structure [4] to produce flame jets aimed toward the eave vents (Fig. 1). Both the target wall and the sheds were underneath a 10 m by 10 m, 20 MW, exhaust hood at NREL [4,21]. The

exhaust collected by this hood leads to an emission control system and an oxygen consumption calorimeter, which measures the heat-release rate (HRR) during an experiment. HRR is often the primary metric of interest for gauging the intensity of the fire. Data from thermocouples (TCs) and additional auxiliary sensors were also collected throughout the burns. Placement of the TCs on the exterior of the wall is shown in Fig. 2 (see Ref. [5] for more information).

In addition, times of important experimental “events” were recorded. These include: “ignition” or the initial ignition time of the source fuel load, “first embers through vent” or the time when embers were first observed entering the interior of the structure via IR or video camera, “vent activation” or the initial time of change seen in the vent (vent closure or half closure), “eave ignition” or the time of ignition for the target structure, and “fire suppression” or the time when water is first applied to the structure.

### 3. SPECTRAL ANALYSIS AND FITTING

Experimental absorption spectra were treated using custom Python and Pascal codes (“PasFireSim”), utilizing spectral parameters and transition information from the HITRAN2020 database [22]. To determine water vapor mole fraction and gas-phase temperature, the photodetector’s raw voltage is first converted to absorbance using the following equation:

$$A(\nu) = -\ln\left(\frac{I}{I_0}\right), \quad (1)$$

where  $A$  denotes absorbance,  $I$  represents the transmitted laser intensity in the presence of the absorbing molecule, and  $I_0$  is the transmitted laser intensity in the absence of an absorber in the optical path (i.e., the background signal). In this study,  $I_0$  was calculated across the full tuning range by performing a linear baseline fit using the 15 data points on either side of the recorded spectrum, where absorption was near zero and variations in the background intensity were approximately linear. For recorded spectra, the background intensity exhibits only slow variations across the scan. Therefore, a linear baseline provides a sufficiently accurate first-order approximation of  $I_0$  while keeping the analysis straightforward. Comparable TDLAS systems with larger scan regions may require a more complex baseline fitting. Both linear and polynomial baselines were evaluated in this work. Fitting residuals showed that more complex polynomials did not improve the quality of the spectral retrievals, and thus the linear model was used. Scans heavily distorted by beam steering or transient particles are rejected by the quality filter prior to fitting (see Section 5.B). For additional information on baseline fit used in this work, see [5], Fig. 49.

Wavenumber calibration of the laser was completed with a wavemeter (manufacturer-specified accuracy of  $\pm 0.028$  nm) and was implemented to convert the recorded laser temperature and current to emitted frequency. Drift in peak location observed throughout the experimental series was within the uncertainty range of the laser controller and wavemeter calibration. Experimental spectra were then fit using a model calculated as

$$A(\nu) = S(T) \cdot g(\nu, P, T) \cdot \rho(P, T) \cdot x \cdot \ell, \quad (2)$$

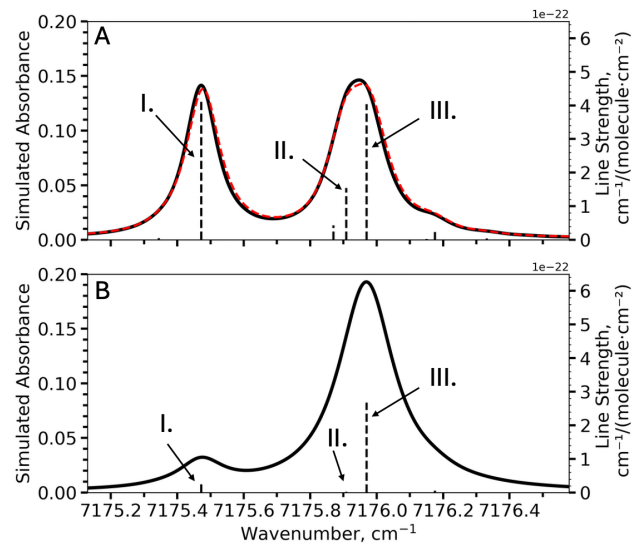


**Fig. 3.** Simulated absorbance spectra (black solid lines using HITRAN database and red dashed lines using HITEMP database) of the sampled region where  $x_{\text{H}_2\text{O}} = 0.010$ ,  $T = 500$  K (A) or  $T = 296$  K (B), at  $P = 1$  atm, and  $\ell = 901$  cm are overlaid with a stick diagram (vertical black dashed lines) of  $\text{H}_2\text{O}$  transitions I, II, and III, which represent temperature-corrected line strengths.

**Table 1.**  $\text{H}_2\text{O}$  Transitions of Interest from  $\nu_1 + \nu_3$  Vibrational Band

Label	Frequency, $\text{cm}^{-1}$	Line Intensity, $\text{cm}^{-1}/(\text{molecule} \cdot \text{cm}^2)$ at 296 K	Lower State Energy, $\text{cm}^{-1}$
I	7175.4930	$2.81 \times 10^{-23}$	1360.2353
II	7175.9220	$2.26 \times 10^{-24}$	2129.5992
III	7175.9873	$2.68 \times 10^{-22}$	206.3014

where  $S(T)$  is the molecular line intensity from the HITRAN [22] or HITEMP [23] database with units of  $\text{cm}^{-1}/(\text{molecule} \cdot \text{cm}^2)$ ,  $g(\nu, P, T)$  is the calculated line profile,  $\rho(P, T)$  is the molecular density,  $x$  is the mole fraction of the target species, and  $\ell$  is the optical path length.  $\nu$  denotes frequency,  $P$  represents pressure, and  $T$  is temperature. For this work, a Voigt line profile was utilized. Both total path lengths were approximately 901 cm, as detailed in Section 3.B.

Figure 3 displays simulated spectra of the two absorption features of interest in this study at a water vapor mole fraction of 0.010. Figure 3(A) shows an extreme example of a simulated spectrum at 500 K using both the HITRAN (black solid line) and the HITEMP (red dashed line) databases, while Fig. 3(B) shows a simulated “background” spectrum at 296 K over a 901 cm path length. The major absorption lines of interest in this region are from the  $\nu_1 + \nu_3$  vibrational band of water. The transitions displayed in Fig. 3 (I–III) are listed in Table 1. The lower state energy of each molecular transition contributes to a unique temperature dependence.

The modeled spectra from PasFireSim were fit to experimental spectra using an Nelder–Mead simplex algorithm to determine water vapor mole fraction and temperature for each spectrum [24]. For the final fits, the HITRAN2020 database was used, as the path-averaged temperatures were lowered

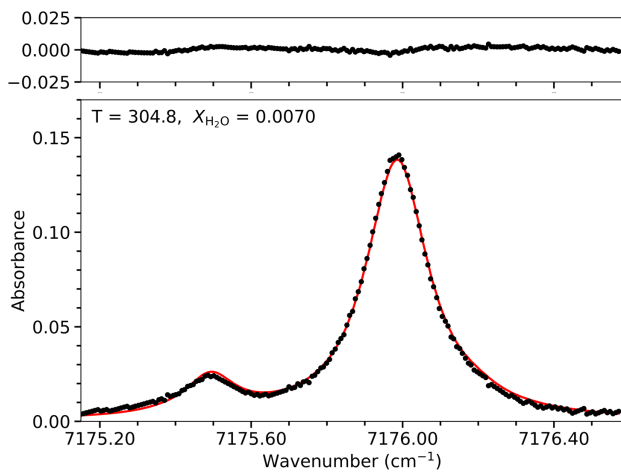


**Fig. 4.** Example experimental spectrum (black dots) and spectral fit (red line) for eaves path collection 1.32 min after fire ignition. Corresponding fit residuals are shown above. The signal-to-noise ratio for this spectrum is 169 with a fit quality factor of 82.04.

relative to peak local temperatures, making HITRAN line intensities more appropriate than HITEMP. Initial values for the temperature were selected by utilizing path-length weighted averaging of auxiliary thermocouple sensors placed on the width of the structure, as illustrated in Fig. 2(B). In Eq. (2), since temperature is being optimized, the line intensity, line profile, and molecular density are recalculated with each step of the simplex. Initial values for the water vapor mole fraction were determined by utilizing auxiliary ambient humidity, temperature, and pressure sensors in the experimental zone on the day of the experimental trial in the NFRL. An example of a fitted spectrum is shown in Fig. 4.

Quality of the spectral fit was quantified by a fit quality factor (QF), defined as

$$QF = \frac{A_{\max}}{\sigma_{\text{residuals}}}, \quad (3)$$

where  $A_{\max}$  denotes the maximum absorbance of the fit spectrum, and  $\sigma_{\text{residuals}}$  is the standard deviation of the fit residuals across the full spectral range. This metric provides a unitless measure of fit quality analogous to signal-to-noise ratio, where higher values indicate a stronger and more reliable fit relative to the residual variability. The QF was calculated for each fit spectrum and used to assess fitting robustness across measurements.

## 4. RESULTS AND DISCUSSION

### A. System Performance

To evaluate the noise performance of the system, an Allan analysis was performed [25]. For this analysis, a single optical path was configured identically to the experimental setup used at NFRL, with a comparable optical path length (approximately 9.2 m), and was probed for approximately 30 minutes under ambient laboratory conditions. The Allan deviation of baseline noise was calculated using averages of 1–100 spectra, and results are shown in Fig. 5. The observed slope of  $-0.467$  in the log–log plot confirms that the system is dominated by random

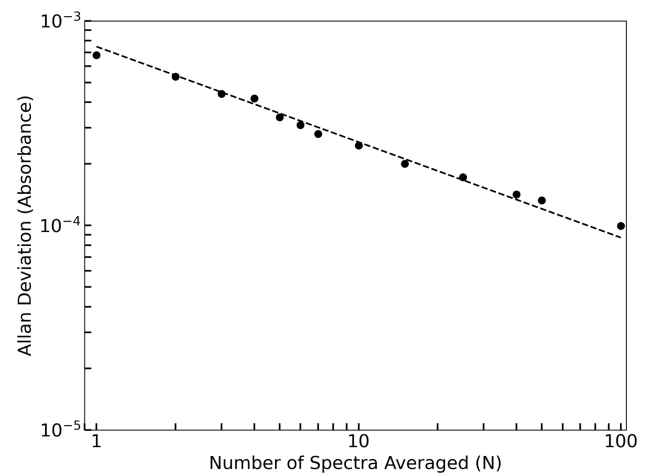


**Fig. 5.** Allan deviation plot for noise along the baseline of absorbance spectra. The dotted line represents a slope of  $-0.467$ , indicative of random noise.

noise across the relevant measurement timescale. The Allan deviation for a single-spectrum acquisition was determined to be  $6.8 \times 10^{-3}$  as shown in Fig. 5. Given the need for temporal resolution of rapid events in a dynamic fire environment and demonstrated high signal-to-noise ratios without averaging, a single-spectrum acquisition approach was adopted for all experiments.

### B. Data Throughput

The open-path instrument was installed at NFRL under the 10 m by 10 m hood from March 2024 to May 2024. During this period, the instrument was used to collect data during twelve experimental burns. The heat release rates (HRRs) of the fires ranged from 700 kW to 2.5 MW as the fuel load (wood cribs) in the source structure (sheds) was varied. Detailed information on HRR for each combination of shed-type and fuel-load is available in [5]. For each burn, the open-path system began data collection prior to ignition, to measure ambient water vapor mole fraction and gas temperature and continued beyond fire suppression.

To facilitate analysis, an initial data quality filter was applied to remove spectra with insufficient signal for fitting (i.e., due to reduced laser transmission observed at the detector or perturbed by interfering particulates). The filter more frequently eliminated data collected from the eaves path, where the laser beam passed directly through flame jets emerging from the source structure toward the eave vent (see Fig. 1). Data throughput, defined as the percentage of total collected spectra as a cumulative pass rate of spectra that pass this quality filter, serves as the proxy for spectral quality, indicating the fraction of the spectra unaffected by signal loss or baseline distortion. In the context of this work, data throughput reflects the tolerance of the system to the multivariate, rapidly evolving conditions of large-scale fire experiments.

The average signal-to-noise (SNR) ratio of the absorbance spectra, calculated as the peak absorbance divided by the baseline noise, exceeded 180. In comparison, the average fit QF, defined in Eq. (3), was 52. This difference is expected, as QF

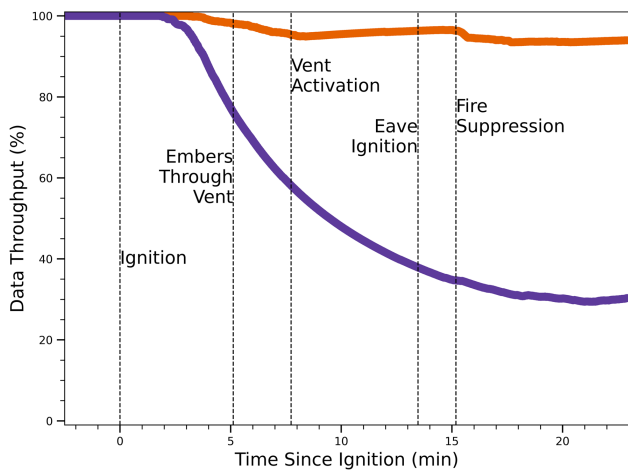


**Fig. 6.** Data throughput for the eaves (purple) and attic (orange) optical paths during an experimental burn (*e10*). Events are demarcated with vertical dashed black lines (see definitions in Section 3.B).

accounts not only for baseline noise but also for structured residuals from baseline drift, minor spectral interferences, or uncertainties in the modeled representations of the spectra. Despite being lower than SNR, QF values remained sufficiently high to indicate robust fits, confirming that the modeled spectra reliably capture the dominant absorption features. Together, the high SNR and strong QF demonstrate the quality of the open-path measurements presented here.

Data throughput and data quality varied throughout each experimental burn. Figure 6 shows an example of data throughput during a single burn, showing a typical pattern: throughput declines in both optical paths following ignition due to increased smoke and flame particulate disrupting laser beam transmission. Following vent activation, throughput in the attic path begins to recover, suggesting that the closing vent helped to block or redirect interfering particles. Additional throughput data from other experimental burns are provided in Supplement 1.

Throughput data quality trends are not isolated, but trends across experiments are difficult to predict due to the multivariate nature of the experimental tests. To better illustrate the complexity of experimental conditions affecting signal quality and data collection, key metrics across all burns are summarized in Table 2. These metrics include the peak HRR of each experimental burn as determined by NFRL (described in Section 3.B) [21], fire suppression time, which represents the burn duration, vent activation status, and the observation of changes in open-path measurements of amount fraction and temperature in response to critical experimental events (discussed in Section 5.C). Notably, tests with longer burn durations and delayed suppression, such as Test ID *e21*, show reductions in throughput percentages, particularly in the eaves path. This is likely due to the sustained burning conditions generating particulates that disrupt the laser beams. Table 2 also captures notable exceptions and data loss events. In Test ID *e15*, for instance, excessive steam during suppression triggered a laser safety shutdown due to prolonged signal loss (Table 2, Notes). Other variables affecting data throughput include fuel load, fuel

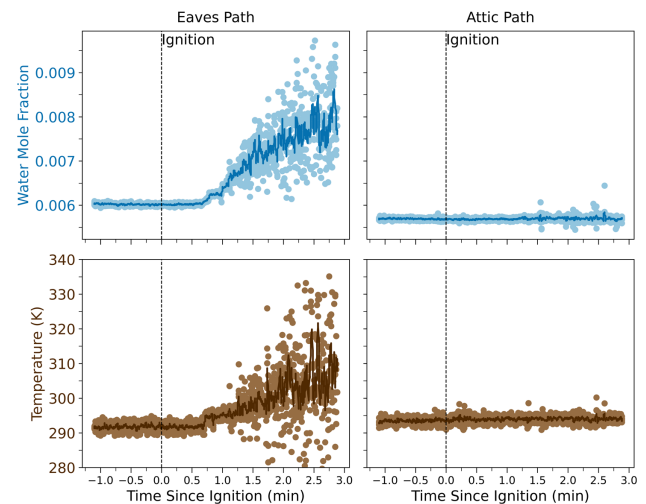


**Fig. 7.** Data from fuel ignition time (black vertical lines) during an experimental burn (*e10*). Left panels show the eaves path, while right panels show the attic path. The top graphs display changes in water vapor mole fraction, and the bottom graphs display changes in temperature in Kelvin. Solid blue and brown lines indicate data smoothed with a Savitsky–Golay filter (15-point window, second-order polynomial).

configuration, various structural changes such as caulking and routing, burn time allowed before suppression, and the location where the structure began to ignite. The effects of these variables on fire spread and vent performance are explored in Ref. [5].

### C. Experimental Data

This section highlights representative portions of the experimental data collected during the burn to highlight the temporal evolution of key measurements, water vapor mole fraction and gas temperature, and the performance of the spectral fitting process based on the path-averaged approach described in Section 4. Two critical events are highlighted: fire ignition and vent activation.

Figure 7 shows data around the time of ignition of one experimental burn (Test ID *e10*). On the left side of Fig. 7, increases in water vapor mole fraction and temperature are observed in the eaves path. On the right side, data from the attic path shows no appreciable changes in these variables at the time of ignition. The behavior in the eaves path aligns with trends observed across all burns, while attic responses were more varied (as noted in Table 2). This variability in the attic response can be attributed to the structural configuration of the target structure. Only approximately 6% of the total optical path in the attic intersects with the flow of hot gases through the eave vent, with most of the path passing through ambient air conditions. This limited interaction zone explains why the attic path measurements are more sensitive to the ambient conditions and showed delayed or absent responses to fire events compared to the eaves path, which passes directly through the active combustion environment (see Section 6.B for further discussion). Additional data from other experimental burns are provided in Supplement 1.

Similarly, Fig. 8 shows data from the attic path around the time of vent activation (Test ID *e10*). After the activation or partial closure of the intumescent eave vent, a notable reduction

**Table 2. Review of Data Throughput and Overall Experimental Results**

Test ID	Peak HRR (MW)	Time of Peak HRR (min) <sup>a</sup>	Vent Closure (Yes, Partial, No)	Time of Fire Suppression (min) <sup>a</sup>	Attic Data Throughput	Eaves Data Throughput	Observed Change within Ignition Window <sup>b</sup>		Observed Change within Vent Activation Window <sup>b</sup>
							Eaves Path	Attic Path	Attic Path
e9	1.1	12.68	Partial	25.02	90 %	25 %	Yes	No	No
e10	1.4	12.85	Partial	15.15	90%	30%	Yes	Yes	Yes
e11	1.4	11.02	Partial	12.47	95%	42%	Yes	Yes	No
e12	0.75	15.45	No	25.03	90%	21%	Yes	Yes	N/A
e13	1.1	8.88	No	25.03	90%	17%	Yes	Yes	N/A
e14	1.3	16.15	No	25.00	50%	17%	Yes	Yes	N/A
e15 <sup>c</sup>	1.7	16.55	Partial	18.93	90%	25%	Yes	Yes	No
e17 <sup>d</sup>	1.4	18.00	Partial	25.02	69%	31%	Yes	N/A	No
e18	1.9	17.98	Partial	18.85	98%	36%	Yes	No	Yes
e19	1.8	15.53	Partial	16.85	84%	31%	Yes	No	Yes
e20	1.4	16.07	Yes	40.00	70%	40%	Yes	No	No
e21	1.4	14.72	Yes	50.10	23%	29%	Yes	Yes	No

<sup>a</sup>Times calculated as minutes since ignition time.

<sup>b</sup>Observable changes which indicate a clear increase or decrease in temperature, water vapor mole fraction, or noise level of the data within specific time windows (see Section 5.C for further discussion and Supplement 1 for additional figures). Ignition window is defined here as one minute prior to and three minutes after fuel ignition. The vent activation window is defined as two minutes before and after the determined vent activation time.

<sup>c</sup>Excessive steam during fire suppression engaged the laser safety shutdown procedure due to prolonged loss of signal at the detector.

<sup>d</sup>Realignment of receiving optics in the attic path prior to this experiment resulted in saturation of the detector and a lower throughput around ignition.

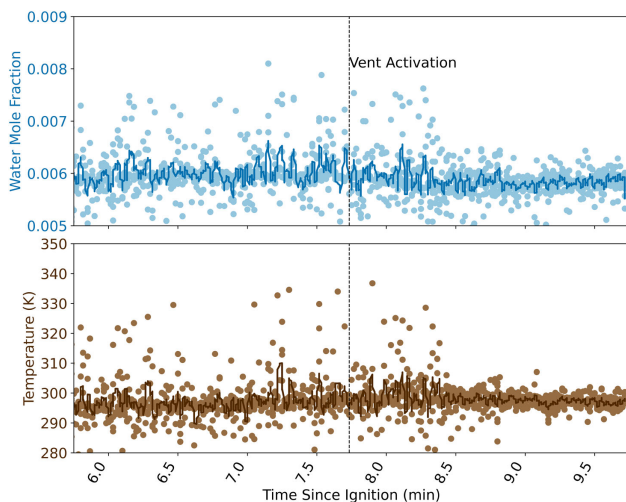


**Fig. 8.** Data from the time of vent activation (black vertical lines) in the attic path (*e10*). The top graph displays changes in water vapor mole fraction, and the bottom graph displays changes in temperature in Kelvin. Solid blue and brown lines indicate data smoothed with a Savitsky–Golay filter (15-point window, second-order polynomial).

of scatter is observed in the fitted spectral results. This reduction likely corresponds to a decrease in interfering particulate and smoke entering the attic path through the eave vent. This trend was common across multiple experiments (such as in Test ID *e18*, see Table 2 and Supplement 1), further emphasizing the attic path’s sensitivity to vent activation and structural configurations. Additional data from other experimental burns are provided in Supplement 1.

#### D. Segmented Spectral Retrieval for Spatial Resolution Enhancement

To enhance spatial resolution along the optical paths and better capture temperature and mole fraction gradients across the structure, we explored the use of a segmented spectral retrieval technique. The method leverages thermocouple measurements distributed along each path to provide initial values for spectral simulations from discrete spatial segments. These segment-specific spectra are then summed and compared to the measured data, with cumulative fit residuals used to optimize the local gas-phase temperature and water vapor mole fraction in each segment.

Figure 9 demonstrates the application of this retrieval strategy using the segment measurements shown in Fig. 2 as black dash-dotted lines. Figures (9A)–(9E) show the simulated spectra for each individual segment along with its corresponding fitted water mole fraction and temperature over their respective path lengths. Compared to traditional path-integrated fitting described in Section 4 and shown in Fig. 4, the segmented approach maintains fit precision with similar fit QF, while providing more spatially resolved profiles of  $x_{H_2O}$  and temperature along the beam path, an advantage for the inhomogeneous fire environments. For example, the path-integrated retrieval of the spectrum shown in Fig. 4, a single integrated temperature of 304.8 K and a water vapor amount fraction of 0.0070 is determined across the full path length, with a QF of 82.04. In contrast, the segmented fit of the same spectrum resolves the temperature gradient and localized increase in water vapor mole fraction. Weighted averages of 304.3 K and 0.00699 for temperature and water vapor mole fraction, respectively, were calculated from the individual segment fits, yielding a nearly identical QF of 82.05. While this segmented approach shows

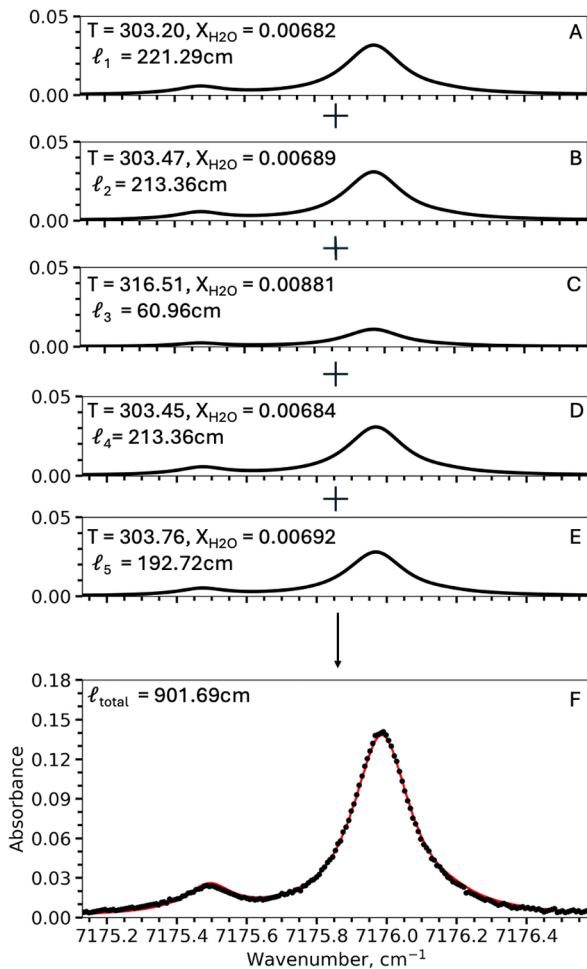


**Fig. 9.** Demonstration of segmented fitting approach applied to the same spectrum shown in Fig. 4, a spectrum collected in the eaves path 1.3 min after ignition. (A)–(E) represent simulated spectra for each distinct path length section, which are combined to generate the total simulated spectra seen as the red solid line in (F). The black data points in (F) represent experimental data. Fit quality factor for this spectrum is 82.05.

promise, its practical application is currently limited by the number and placement of additional auxiliary sensors, like more spatially distributed thermocouples, to provide accurate initial estimates for each segment, which are critical for convergence of fits. With only a sparse distribution of auxiliary sensors, localized spectral features are not fully captured. Expanding the sensor network along each optical path would be necessary to improve the reliability of this approach, but it offers significant diagnostic value that could be used to better identify localized features such as vent-driven flows or hot spots.

Though only the HITRAN database was used in this example due to the lower temperatures in all segments, for applications involving higher-temperature segments, use of the HITEMP database would be recommended to ensure accurate line intensities and temperature-dependent absorption features.

This type of segmented spectral fitting has seen success in atmospheric remote sensing [26,27], and its adaptation as described here could offer a promising path for fire diagnostics. Specifically, this strategy could yield space- and time-resolved

information that could support validation of computational fluid dynamics (CFD) fire models [4,28,29] by providing high-resolution profiles of gas distributions and temperature gradients, particularly in enclosed structures.

## 5. CONCLUSIONS

### A. System Performance and Experimental Findings

In this paper, we have demonstrated the development and installation of an open-path tunable diode laser absorption system for determining gas-phase temperature and water vapor mole fraction along two distinct, simultaneous measurement paths during structure-to-structure fire spread experiments. Among the spectra that pass the analysis quality filter, the system achieved an average SNR above 180, even in this challenging fire environment.

The instrument performed reliably throughout the experimental series and provided quality measurements under the various conditions. The simultaneous dual-path measurements across both the attic and eaves path captured variations in temperature and water vapor as burn “events” progressed. While the eaves path showed strong signal changes throughout the burns, the attic path, due to its limited overlap with fire-affected regions, yielded more static results. These observations underscore the importance of complementary sensor placement, temporal resolution, and test structure design.

### B. Pathways for Instrument and Experimental Improvement

The TDLAS system provided a robust optical and electronic design; however, the data acquisition rate (7 Hz) was constrained by communication latency between the custom control software and the data acquisition hardware. While sufficient to resolve key events in the structural fire experiments presented here, prior work has shown that faster update rates may help to further mitigate the spectral distortion effects of smoke interference and beam steering [30]. These improvements would enable more effective temporal averaging and enhance SNR. In addition to generally faster full-spectrum scanning, higher spectral acquisition rates can be achieved by reducing the number of data points collected per scan, provided that spectral coverage remains sufficient to resolve and fit the relevant absorption features.

In addition to improving acquisition speed, expanding the system’s capabilities to include multi-species detection would significantly enhance its diagnostic power. This instrument was optimized for H<sub>2</sub>O detection using three temperature-sensitive absorption transitions (see Fig. 3). For instance, integrating a second NIR diode or transitioning to a mid-IR laser would allow for simultaneous (or near-simultaneous) CO<sub>2</sub> and H<sub>2</sub>O measurements. Spectra collected around 2.7 μm show absorption lines of these two gases within 0.22 cm<sup>-1</sup> of each other with similar line strengths, which would make them a promising target for dual detection [31,32]. The CO<sub>2</sub> transition in this region exhibits strong temperature dependence due to its high *J* level (*J*'' = 34) and the Boltzmann population distribution, which enhances sensitivity to temperature variations that would be beneficial for dynamic fire diagnostics.

Complementary to these hardware improvements, modifications to the test structure itself could further improve the sensitivity of the laser-based measurements. As detailed in the fire dynamics simulations in Ref. [4], Appendix E, a partially or fully enclosed attic space would allow for gas retention and more pronounced temperature gradients, spatially and temporally. In the current setup, only a small portion (approximately 6%) of the total attic optical path was influenced by the flow of hot gases and particulates through the eave vent.

Overall, this work demonstrates that TDLAS measurements can be robust in large-scale fire experiments and highlights several key design and instrumentation considerations for future deployments. Accurate interpretation of the quantitative results from the data requires recognition of the inherently stochastic nature of large-scale burns with a complex multivariate testing matrix. The capability to obtain gas-phase information under harsh conditions, without perturbing the local environment, provides valuable insights into fire dynamics and gas transport in structure scale burns, which act as the closest analogs to real-world fires. Continued refinement of acquisition speed, multi-species capabilities, and usage of more spatially resolved retrieval methods can further extend the utility of this platform, enabling improved validation of fire models and fire safety engineering aimed at enhancing structure resilience in WUI fires.

**Funding.** National Institute of Standards and Technology; National Science Foundation (CBET-2412623); National Aeronautics and Space Administration (NNX14AN89G).

**Acknowledgment.** Support for EEMc for Summer 2024 was provided by the NIST Professional Research Experience Program (PREP). Additional partial salary support for EEMc and JHM was provided by the US National Science Foundation through grant CBET-2412623, and partial support for some of the laboratory equipment was provided by NASA Hydrospheric and Biospheric Science Research Program (Grant/Cooperative Agreement Number NNX14AN89G). The authors would like to thank the staff of the National Fire Research Laboratory for enabling the successful integration of the open-path system in the high-bay test area. Additional information about the full description of the technical plan, test matrix, and experimental approaches can be found in a published Technical Note (doi.org/10.6028/NIST.TN.2288) and Report (doi.org/10.6028/NIST.TN.2341). Certain instruments are identified in this paper in order to specify the experimental procedure adequately. Such identification is not intended to imply recommendation or endorsement by NIST, nor is it intended to imply that the instruments identified are necessarily the best available for the purpose.

**Disclosures.** The authors declare that they have no relevant or material financial interests that relate to the research described in this paper.

**Data availability.** Data underlying the results presented in this paper are available in Ref. [33].

**Supplemental document.** See Supplement 1 for supporting content.

## REFERENCES

- National Interagency Fire Center, "Statistics|Wildfires and Acres," <https://www.nifc.gov/fire-information/statistics/>.
- National Aeronautics and Space Administration, "Global surface temperature|NASA global climate change," <https://climate.nasa.gov/vital-signs/global-temperature?intent=121>.
- M. Burke, A. Driscoll, S. Heft-Neal, *et al.*, "The changing risk and burden of wildfire in the United States," *Proc. Natl. Acad. Sci.* **118**, e2011048118 (2021).
- C. U. Brown, A. Maranghides, S. Nazare, *et al.*, "NIST Eave and Vent Experiments (EaVE) EaVEs phase a: test plan," Tech. Note 2288 (National Institute of Standards and Technology (U.S.), 2024).
- C. U. Brown, A. Maranghides, S. Nazare, *et al.*, "NIST Eave and Vent Experiments (EaVE) EaVEs: Phase A," Tech. Note 2341 (National Institute of Standards and Technology (U.S.), 2025).
- International Code Council, "2022 California Building Code, Title 24, Part 2 (Volumes 1 & 2) with July 2024 Supplement updated, Chapter 7A Materials and construction methods for exterior wildfire exposure," (2022).
- S. Ghanekar, R. Rajasegar, N. Traina, *et al.*, "In-situ measurement of water-vapor in fire environments using a real-time tunable diode laser based system," *Fire Saf. J.* **120**, 103114 (2021).
- R. S. Parmar, M. Welling, M. O. Andreae, *et al.*, "Water vapor release from biomass combustion," *Atmos. Chem. Phys.* **8**, 6147–6153 (2008).
- G. L. Achtemeier, "Measurements of moisture in smoldering smoke and implications for fog," *Int. J. Wildland Fire* **15**, 517–525 (2006).
- Vaisala, "Response time in humidity measurement," Tech Note. B211803EN-B (Vaisala, 2021).
- S. R. Tieszen, "On the fluid mechanics of fires," *Annu. Rev. Fluid Mech.* **33**, 67–92 (2001).
- M. J. Hurley, D. T. Gottuk, J. R. Hall, Jr., *et al.*, *SFPE Handbook of Fire Protection Engineering* (Springer, 2015).
- J. Wang and H. Wang, "Tunable fiber laser based photoacoustic gas sensor for early fire detection," *Infrared Phys. Technol.* **65**, 1–4 (2014).
- J. Dang, H. Yu, C. Zheng, *et al.*, "An early fire sensor based on infrared gas analytical methods," *Anal. Methods* **10**, 3325–3331 (2018).
- B. Yu, X. Wu, M. Zhang, *et al.*, "Tunable diode laser absorption spectroscopy for open-path monitoring gas markers in fire combustion products," *Infrared Phys. Technol.* **131**, 104690 (2023).
- C. R. Shaddix, S. W. Allendorf, G. L. Hubbard, *et al.*, *Diode Laser Diagnostics for Gas Species and Soot in Large Fires: LDRD Project Final Report* (Sandia National Lab. (SNL-NM), Sandia National Lab. (SNL-CA), 2001).
- W. VonDrasek and A. Melsio-Pubill, *Tunable Diode Laser Sensor for Monitoring and Control of Harsh Combustion Environments* (American Air Liquide, 2006).
- H. Teichert, T. Fernholz, and V. Ebert, "Simultaneous in situ measurement of CO, H<sub>2</sub>O, and gas temperatures in a full-sized coal-fired power plant by near-infrared diode lasers," *Appl. Opt.* **42**, 2043–2051 (2003).
- K. Hinnant, M. Lee, A. Davis, *et al.*, "Comparative measurements of TDLAS and multi-gas sensor to monitor fire extinction inside small-scale backdraft compartment using CO<sub>2</sub> and CO concentrations," *Fire Technol.* **61**, 5939–5958 (2025).
- D. M. Bailey, E. M. Adkins, and J. H. Miller, "An open-path tunable diode laser absorption spectrometer for detection of carbon dioxide at the Bonanza Creek Long-Term Ecological Research Site near Fairbanks, Alaska," *Appl. Phys. B* **123**, 245 (2017).
- R. A. Bryant and M. F. Bundy, "The NIST 20 MW calorimetry measurement system for large-fire research," Tech. Note 2077 (National Institute of Standards and Technology, 2019), paper NIST TN 2077.
- I. E. Gordon, L. S. Rothman, R. J. Hargreaves, *et al.*, "The HITRAN2020 molecular spectroscopic database," *J. Quant. Spectrosc. Radiat. Transf.* **277**, 107949 (2022).
- L. S. Rothman, I. E. Gordon, R. J. Barber, *et al.*, "HITEMP, the high-temperature molecular spectroscopic database," *J. Quant. Spectrosc. Radiat. Transf.* **111**, 2139–2150 (2010).
- J. Nelder and R. Mead, "A simplex method for function minimization," *Comput. J.* **7**, 308–313 (1965).
- P. Werle, R. Mücke, and F. Slemr, "The limits of signal averaging in atmospheric trace-gas monitoring by tunable diode-laser absorption spectroscopy (TDLAS)," *Appl. Phys. B* **57**, 131–139 (1993).
- M. M. Flores, D. S. Bomse, and J. H. Miller, "Statistical characterization of temperature and pressure vertical profiles for the analysis of laser heterodyne radiometry data," *Sensors* **21**, 5421 (2021).
- D. S. Bomse, J. E. Tso, M. M. Flores, *et al.*, "Precision heterodyne oxygen-corrected spectrometry: vertical profiling of water and carbon dioxide in the troposphere and lower stratosphere," *Appl. Opt.* **59**, B10–B17 (2020).

28. K. McGrattan, S. Hostikka, R. McDermott, *et al.*, “Fire dynamics simulator user’s guide,” NIST Special Publication 1019, 1–339 (National Institute of Standards and Technology, 2013).
29. X. Sanchez-Monroy, W. Mell, J. Torres-Arenas, *et al.*, “Fire spread upslope: numerical simulation of laboratory experiments,” *Fire Saf. J.* **108**, 102844 (2019).
30. E. W. Mitchell, M. S. Hoehler, F. R. Giorgetta, *et al.*, “Coherent laser ranging for precision imaging through flames,” *Optica* **5**, 988–995 (2018).
31. A. Pogány, S. Wagner, O. Werhahn, *et al.*, “Development and metrological characterization of a tunable diode laser absorption spectroscopy (TDLAS) spectrometer for simultaneous absolute measurement of carbon dioxide and water vapor,” *Appl. Spectrosc.* **69**, 257–268 (2015).
32. A. K. Mohamed, J. Messineo, J.-Y. Lestrade, *et al.*, “Tunable diode laser absorption spectroscopy of CO<sub>2</sub> and H<sub>2</sub>O at 2.7 μm in a scramjet combustor and in exhaust gases of a hybrid rocket motor,” in *32nd AIAA Aerodynamic Measurement Technology and Ground Testing Conference, AIAA AVIATION Forum* (American Institute of Aeronautics and Astronautics, 2016).
33. E. McCaughey, M. Flores, C. Brown, *et al.*, “Data for ‘Demonstration of near-infrared open-path absorption spectroscopy for water vapor and temperature monitoring during structure-to-structure fire spread experiments’,” Version 1.0, NIST Public Data Repository (2026), <https://doi.org/10.18434/mds2-4029>.